

# Digital spiral imaging

Lluís Torner and Juan P. Torres

*ICFO-Institut de Ciències Fotoniques, and Department of Signal Theory and Communications, Universitat Politècnica de Catalunya, 08034 Barcelona, Spain*

[Lluís.Torner@icfo.es](mailto:Lluís.Torner@icfo.es)

Silvia Carrasco

*Quantum Imaging Laboratory, Department of Electrical & Computer Engineering and Department of Physics, Boston University, 8 Saint Mary's Street, Boston, Massachusetts 02215, USA*

**Abstract:** A major application of optics is imaging all types of structural, physical, chemical and biological features of matter. Techniques based on most known properties of light have been developed over the years to remotely acquire information about such features. They include the spin angular momentum, encoded in the polarization, but not yet the orbital angular momentum encoded in its spiral spectrum. Here we put forward the potential of such spiral spectra. In particular, we use several canonical examples to show how the orbital angular momentum spectra of a light beam can be used to image a variety of intrinsic and extrinsic properties encoded, e.g., in phase and amplitude gradients, dislocations or delays.

© 2005 Optical Society of America

**OCIS codes:** (110.0110) Imaging Systems; (120.0120) Instrumentation, Measurement and Metrology; (170.0170) Medical Optics and Biotechnology; (260.0260) Physical Optics; (270.0270) Quantum Optics; (280.0280) Remote Sensing

---

## References and links

1. L. Allen, M. J. Padgett and M. Babiker, "The orbital angular momentum of light," *Progress in Optics* **39**, 291-372 (1999).
2. M. J. Padgett, J. Courtial, and L. Allen, "Light's Orbital Angular Momentum," *Phys. Today* **57**, 35-40 (2004).
3. C. Cohen-Tannoudji, J. Dupont-Roc, and G. Grynberg, *Photons and Atoms: Introduction to Quantum Electrodynamics* (Wiley, New York, 1989).
4. S. M. Barnett, "Optical angular-momentum flux," *J. Opt. B* **4**, S7-S16 (2002).
5. A. T. Neil, I. MacVicar, L. Allen, M. J. Padgett, "Intrinsic and extrinsic nature of the orbital angular momentum of a light beam," *Phys. Rev. Lett.* **88**, 053601 (2002).
6. L. Paterson, M. P. MacDonald, J. Arlt, W. Sibbett, P. E. Bryant, and K. Dholakia, "Controlled rotation of optically trapped microscopic particles," *Science* **292**, 912-914 (2001).
7. N. B. Simpson, K. Dholakia, L. Allen, and M. Padgett, "Mechanical equivalence of spin and orbital angular momentum of light: an optical spanner," *Opt. Lett.* **22**, 52-54 (1997).
8. H. He, M. E. J. Friese, N. R. Heckenberg, and H. Rubinsztein-Dunlop, "Direct observation of transfer of angular momentum to absorbing particles from a laser beam with a phase singularity," *Phys. Rev. Lett.* **75**, 826-829 (1995).
9. N. R. Heckenberg, T. A. Nieminen, M. E. J. Friese, and H. Rubinsztein-Dunlop, "Trapping microscopic particles with singular beams," in *International Conference on Singular Optics*, M. S. Soskin ed., Proc. SPIE **3487**, 46-53 (1998).
10. P. Galajda and P. Ormos, "Complex micromachines produced and driven by light," *Appl Phys. Lett.* **78**, 249-251 (2001).
11. G. Swartzlander, "Peering into darkness with a vortex spatial filter," *Opt. Lett.* **26**, 497-499 (2001).
12. E. Santamato, A. Sasso, B. Piccirillo, and A. Vella, "Optical angular momentum transfer to transparent isotropic particles using laser beam carrying zero average angular momentum," *Opt. Express* **10**, 871-878 (2002).  
<http://www.opticsexpress.org/abstract.cfm?URI=OPEX-10-17-871>

13. D. G. Grier, "A revolution in optical manipulation," *Nature (London)* **424**, 810-816 (2003).
14. K. Dholakia, G. Spalding, and M. MacDonald, "Optical tweezers: the next generation," *Physics World* **15**, 31 (2002).
15. K. Dholakia, H. Little, C. T. A. Brown, B. Agate, D. McGloin, L. Paterson, and W. Sibbett, "Imaging in optical micromanipulation using two-photon excitation," *New J. Phys.* **6**, 136 (2004).
16. E. Santamato, "Photon orbital angular momentum: problems and perspectives," *Fortschr. Phys.* **52**, 1141-1153 (2004).
17. A. Mair, A. Vaziri, G. Weihs, and A. Zeilinger, "Entanglement of the orbital angular momentum states of photons," *Nature (London)* **412**, 313-316 (2001).
18. G. Molina-Terriza, J. P. Torres, and L. Torner, "Management of the angular momentum of light: preparation of photons in multidimensional vector states of angular momentum," *Phys. Rev. Lett.* **88**, 013601 (2002).
19. A. Vaziri, G. Weihs and A. Zeilinger, "Experimental two-photon, three-dimensional entanglement for quantum communication," *Phys. Rev. Lett.* **89**, 240401 (2002).
20. M. S. Soskin and M. V. Vasnetsov, "Singular Optics," *Progress in Optics* **42**, 219-276 (2001).
21. E. G. Johnson, J. Stack, and Ch. Koehler, "Light coupling by a vortex lens into graded index fiber," *J. Lightwave Technol.* **19**, 753-758 (2001).
22. C. Rockstuhl, M. Salt, and H. P. Herzing, "Theoretical and experimental investigation of phase singularities generated by optical micro- and nano-structures," *J. Opt. A* **6**, S271-S276 (2004).
23. R. J. Voogd, M. Singh, S. Pereira, A. van de Nes, and J. Braat, "The use of orbital angular momentum of light beams for super-high density optical data storage," OSA Annual Meeting, Rochester, NY, October 2004, paper FTuG14.
24. M. M. Varma, D. D. Nolte, H. D. Inerowicz, and F. E. Regnier, "Spinning-disk self-referencing interferometry of antigen-antibody recognition," *Opt. Lett.* **29**, 950-952 (2004).

## 1. Introduction

A major application of optics is imaging and probing structural, physical, chemical and biological properties of matter. Therefore, a rich variety of techniques for remote imaging based on most known classical and quantum properties of light have been elucidated and developed over the years. Available techniques rely in the exploitation of all types of spatial, temporal, vectorial, and nonlinear interactions of light with matter. Traced back to the fundamental properties of light, the known techniques rely on a particular use of the energy, the energy spectra and the energy density of light signals, their longitudinal and transverse linear momenta, their temporal and spatial coherence, and their angular momentum associated to the polarization of the electromagnetic fields.

However, the angular momentum can contain not only a *spin* contribution associated to the polarization, but also an *orbital* contribution associated to the spatial profile of the light beam amplitude and phase-front [1, 2]. Within the paraxial regime, both contributions can be measured and manipulated separately [3]-[5], and the orbital contribution is finding important applications in fields that range from optical tweezing in biosciences, to microfluidics, micromechanics, and quantum information (see, e.g., [6]-[19], and references therein). Nevertheless, while the spin angular momentum is a workhorse in imaging across the electromagnetic spectrum, the orbital angular momentum spectrum has not yet been added to the toolkit. Our aim in this paper is to illustrate the potential of the spiral spectra of light beams for remotely image suitable features of matter.

The concept we put forward comprises illuminating the target with a light beam with a convenient spatial shape, expanding the reflected or transmitted signal into the spiral eigenstates of orbital angular momentum, and acquiring information of the target by analyzing the corresponding spiral spectrum [18]. The shape of the spiral spectrum, its bandwidth, or the weights of prescribed eigenstates carry the sought after information. A principal difference between the spin angular momentum and the orbital angular momentum is that the former forms two-dimensional light states (e.g., vertical or horizontal polarization) while the latter encodes information in infinite-dimensional states, hence providing multi-dimensional acquisition alphabets. Also, while the spin angular momentum manifests itself in the vectorial nature of the light fields

and is thus particularly sensitive to material anisotropies, the orbital angular momentum can be associated to the topological properties of the light wavefront and hence is specially sensitive to phase gradients and discontinuities. Both features open a wealth of new opportunities to gain information from suitable targets.

## 2. Concept

Light carrying orbital angular momentum can be described in terms of Laguerre-Gaussian (LG) modes which contain an  $\exp(im\varphi)$  term describing an on-axis phase singularity of strength  $m$ . In addition to the index  $m$ , which can take any integer number and determines the azimuthal phase dependence of the mode, the LG modes are also characterized by an index  $p$ , which can take any non-negative value and determines the radial shape, or node number, of the light distribution. The normalized  $LG_{m,p}$  mode at its beam waist is given in cylindrical coordinates by

$$LG_{m,p}(\rho, \varphi) = \left( \frac{2p!}{\pi(|m|+p)!} \right)^{1/2} \frac{1}{\eta} \left( \frac{\sqrt{2}\rho}{\eta} \right)^{|m|} L_p^{|m|} \left( \frac{2\rho^2}{\eta^2} \right) \exp\left(-\frac{\rho^2}{\eta^2}\right) \exp(im\varphi), \quad (1)$$

where  $L_p^m$  are the associated Laguerre polynomials,  $\rho$  is the radial cylindrical coordinate,  $\varphi$  is the azimuthal angle, and  $\eta$  is the beam waist.

The LG modes form a complete, infinite-dimensional basis for the solutions of the paraxial wave equation; thus any field distribution can be represented as a vector state in that basis. When  $m \neq 0$ , the LG modes contain screw wave-front dislocations, or optical vortices [20], with topological charge or winding number  $m$ . Their intensity cross-sections consist of a radially symmetric shape with no on-axis intensity (Fig. 1). The width of the LG mode increases with the value of the index  $m$ . Thus, the maximum value of  $m$  that may be used is only restricted by the finite apertures of the actual optical system.

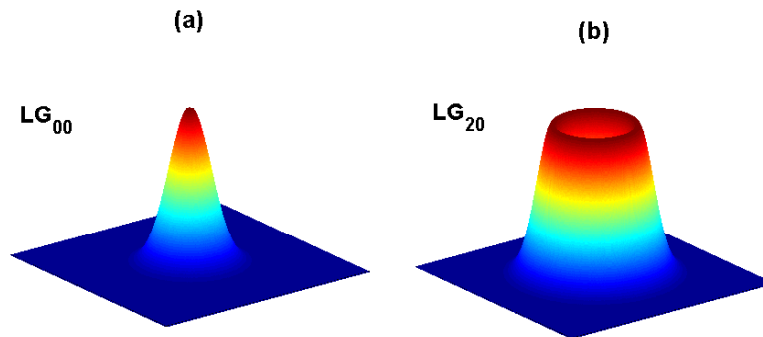


Fig. 1. Intensity distribution of two different LG modes: (a)  $LG_{00}$  ( $m = 0$ ,  $p = 0$ ), and (b)  $LG_{20}$  ( $m = 2$ ,  $p = 0$ ).

Consider the slowly varying electric field envelope  $u(x, y; z)$  of a continuous wave paraxial beam propagating in the  $z$  direction, where  $x$  and  $y$  are the transverse coordinates. The time averaged energy per unit length carried by the beam is  $U = 2\epsilon_0 \iint |u|^2 dx dy$ , where  $\epsilon_0$  is the permittivity of vacuum. The time averaged  $z$  component of the orbital angular momentum per

unit of length carried by the light beam is given by:  $L_z = \int \int [\vec{r}_\perp \times \vec{p}] dx dy$ , where  $\vec{r}_\perp$  is the vector position in the  $X$ - $Y$  plane,  $\vec{p} = (i\epsilon_0/\omega) [u \nabla_\perp u^* - u^* \nabla_\perp u]$ , and  $\omega$  is the angular frequency.

To elucidate the orbital angular momentum content, or spiral spectrum, of a field distribution  $u(x, y; z)$  one has to compute its projection into the spiral harmonics  $\exp(in\varphi)$ , since, for a given winding number  $n$ , we have to add the weights of all LG modes with the same index  $n$ , independently of the index  $p$ . We thus let

$$u(\rho, \varphi; z) = \frac{1}{\sqrt{2\pi}} \sum_{n=-\infty}^{n=\infty} a_n(\rho, z) \exp(in\varphi), \quad (2)$$

where  $a_n = 1/(2\pi)^{1/2} \int_0^{2\pi} u(\rho, \varphi, z) \exp(-in\varphi) d\varphi$ . The energy carried by the corresponding light beam can be written as  $U = 2\epsilon_0 \sum_{n=-\infty}^{\infty} C_n$ , where  $C_n = \int_0^\infty |a_n(\rho, z)|^2 \rho d\rho$ , can be shown to be a constant independent of  $z$ . The angular momentum of the light beam is thus given by  $L_z = (2\epsilon_0/\omega) \sum_{n=-\infty}^{\infty} nC_n$ . The energy content (weight) of each of the spiral harmonics of any field distribution in the paraxial regime of light propagation is then determined by:

$$P_n = \frac{C_n}{\sum_{q=-\infty}^{\infty} C_q} \quad (3)$$

Standard imaging techniques extract information from a target translating the sought after property into changes in the intensity, phase, frequency via nonlinear processes excitation, polarization or the spatial distribution of an input beam. The input beam can be a Gaussian beam or a beam with certain intensity, polarization or phase distribution. The concept we put forward here, which might be termed *spiral spectrally-resolved imaging* or *spiral imaging* in short, comprises illuminating a target with a light beam with a convenient spatial shape, expanding the reflected or transmitted signal into the spiral eigenstates of orbital angular momentum, and acquiring information of the target by analyzing the weights of prescribed eigenstates in the detected signal.

Consider a general illuminating field  $u_0(\rho, \varphi, z)$  with a defined spiral spectral decomposition. This input beam can be a pure LG mode, or a combination of modes. Reflecting or transmitting the beam by a target with a certain transfer function which depends on the transverse coordinates  $R(\rho, \varphi)$  causes the output field, given by  $u_{out}(\rho, \varphi, z) = R(\rho, \varphi)u_0(\rho, \varphi, z)$ , to vary depending on the physical properties of the target. Such variation directly translates into changes into the spiral spectrum. Thus, the difference between the input and output spiral content contains information about the transfer function of the target. To illustrate the potential of the concept, here we address a few canonical examples.

### 3. Discussion

First, let a target imprint a  $\phi$ -phase dislocation across the center of the illuminating beam. This is similar to the case encountered, for example, in standard compact disc-reading where an on-axis Gaussian beam illuminates partially a pit and partially the land. Adjusting adequately the height of the pit leads to a phase difference between both parts of the reflected beam of  $\phi = \pi$ . Let a collimated Gaussian beam, i.e., a pure  $n = 0$  line in the spiral spectrum, illuminate such target. Figure 2 shows the spiral spectrum of the output field. Notice that about 82% of the output energy is carried by the  $n = \pm 1$  sidelobes.

Variations of the path length in the region of the dislocation affect  $\phi$ , a possibility that might be used to detect minute variations of the physical or the effective strength of the dislocation (i.e., the physical height in the case of reflective pits or the effective height in the case of transparent pits). Figure 3(a) summarizes the impact of such phase delay variation in the spiral spectrum in a few illustrative cases. Figure 3(b) shows the weight of the central ( $n = 0$ ) and

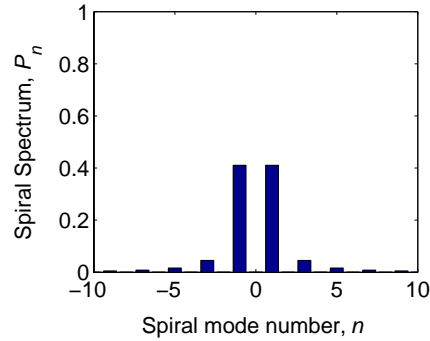


Fig. 2. Spiral spectra of the output field reflected/refracted from a target imprinting a  $\pi$  phase dislocation across in the center of the illuminating beam. The transfer function of such a target has the form:  $R(x,y) = 1$  for  $x < 0$ , and  $R(x,y) = -1$  otherwise. The input field is a Gaussian beam (pure  $LG_{00}$  mode).

the first adjacent sidelobes ( $n = \pm 1$ ) of the output beam versus the phase delay. Notice the monotonic variation of the weights of the sidelobes versus the path delay.

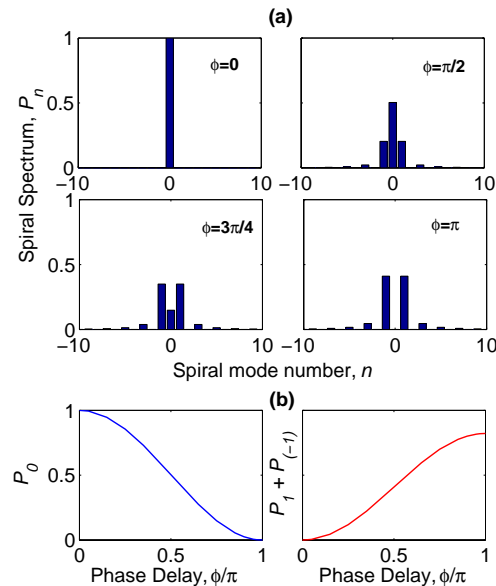


Fig. 3. (a) Spiral spectra of the output field reflected/refracted from a target imprinting a  $\phi$  phase dislocation across in the center of the illuminating beam for four selected values of the phase dislocation. (b) Weight of the central ( $n = 0$ ),  $P_0$  and the first adjacent ( $n = \pm 1$ ) sidelobes,  $P_1 + P_{(-1)}$  versus the normalized phase dislocation  $\phi/\pi$ . The transfer function of the target has the form:  $R(x,y) = 1$  for  $x < 0$ , and  $R(x,y) = e^{i\phi}$  otherwise. The input field is a Gaussian beam.

The spiral spectrum can also be used to gain quantitative information about the position of the phase dislocation. This is shown in Fig. 4, which displays the variation of the spiral spectra of the output beam obtained when a Gaussian beam illuminates an off-axis  $\pi$  phase-jump, for different positions of the dislocation.

The above examples rely on the variation of narrowband data (i.e., weights of a few modes)

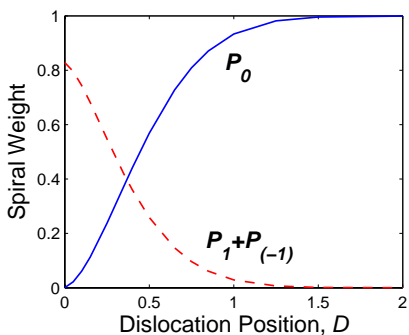


Fig. 4. Weight of the central ( $n = 0$ ),  $P_0$  and the first adjacent ( $n = \pm 1$ ) sidelobes,  $P_1 + P_{(-1)}$  for a Gaussian beam of beam waist  $\eta = 1$  illuminating an off-axis  $\pi$  phase dislocation placed at a distance  $D$  from the center of the beam.

to gain information about the properties of the target. However, broadband outputs are also useful. For example, a property that provides information is the output spiral bandwidth, i.e., the width of the spiral spectrum of the generated field. An illustrative example is shown Fig. 5, which displays the spiral content produced by different combs of  $\pi$  edge-dislocations. The impact of the separation between edges in the comb on the spiral bandwidth is clearly visible.

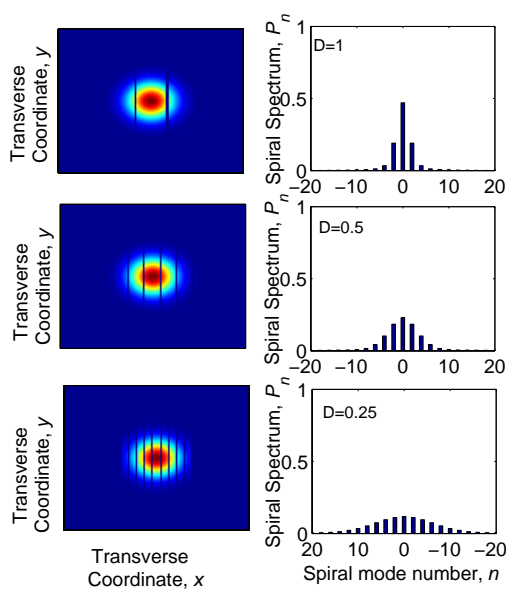


Fig. 5. Output intensity distributions (left column), and spiral spectra (right column) for a Gaussian beam of beam waist  $\eta = 1$  illuminating a target imprinting a comb of  $\pi$  phase dislocations. Each row displays a different value  $D$  of the separation between the edges. Top row,  $D = 1$ ; middle row,  $D = 0.5$ ; bottom row,  $D = 0.25$ .

The previous targets feature phase dislocations, phase discontinuities and edges. Continuous phase (or amplitude) gradients might be also imaged by monitoring the spiral spectrum that they produce. Two different examples are shown in Figs. 6 and 7, for targets with transfer functions featuring phase gradients with the form  $\exp(i\alpha\pi x/\eta)$ , and  $\exp(i\alpha\pi|x|/\eta)$ , respectively. One important result is that while both gradients generate similar broadband outputs, with a

bandwidth directly linked to the value of the strength  $\alpha$ , in the case of the antisymmetric phase gradient all types of modes are excited, whereas in the case of the symmetric gradient all odd sidelobes are suppressed.

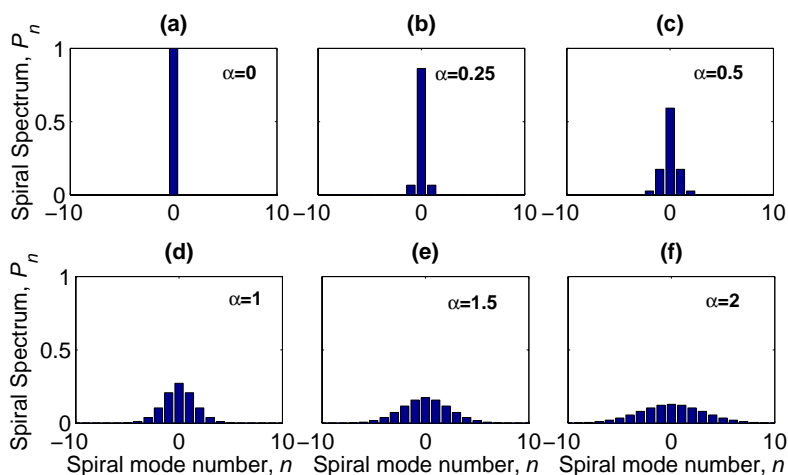


Fig. 6. Spiral spectra of the output field for a Gaussian beam of beam waist  $\eta = 1$  illuminating a target featuring an antisymmetric phase gradient across the input beam for different selected strengths  $\alpha$  of the phase gradient. The transfer function of the target has the form  $R(x,y) = e^{i\alpha\pi x/\eta}$ .

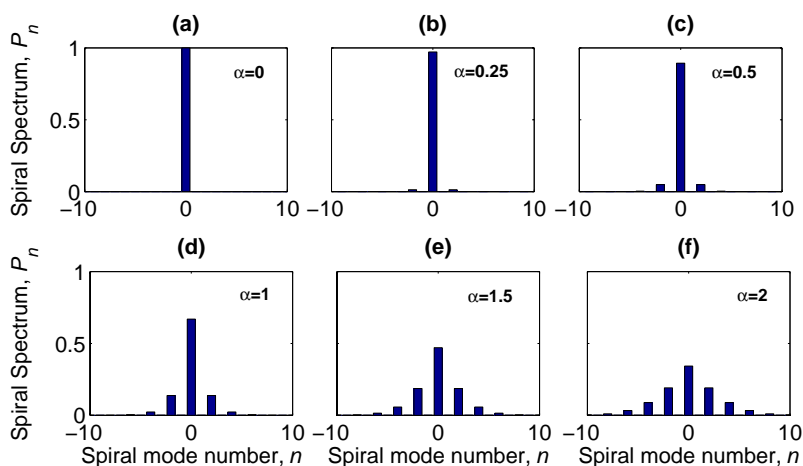


Fig. 7. Same as in Fig. 6, for a symmetric phase gradient target of the form  $R(x,y) = e^{i\alpha\pi|x|/\eta}$ .

The idea behind spiral imaging holds not only for transfer functions that feature variations in phase, but also for transfer functions with amplitude inhomogeneities of different sorts. For example, Fig. 8 illustrates the case of a perfectly reflecting structure consisting of a blocking strip of different widths that stops the beam at its center along one of the axes. Again changes of the position, shape, and number of strips are translated in changes into the spiral spectrum. In this plot, we used an illuminating beam in the form of a LG mode of winding number  $m = 2$ ,

to stress that using illuminating beams with an optimized, or engineered, spiral spectrum is an important aside possibility open also for exploration.

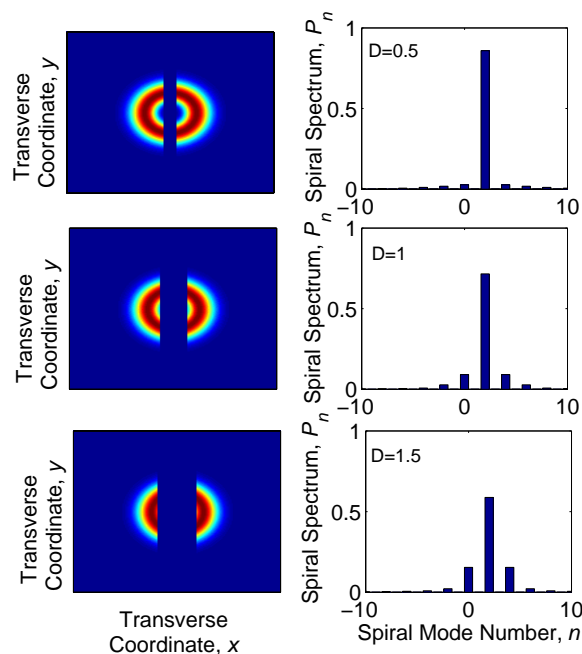


Fig. 8. Intensity distributions (left column), and spiral spectra (right column) of the output field reflected from a perfect mirror with a blocking strip of different widths  $D$  placed in the center of the illuminating beam. The transfer function of such a target has the form  $R(x,y) = 1$  for  $|x| > D/2$ , and  $R(x,y) = 0$  otherwise. The input beam is a pure LG mode with  $m = 2$ , and a beam waist  $\eta = 1$ .

It is worth emphasizing that the information acquired by this scheme is not only geometrical. Because of the very nature of the orbital angular momentum, the spiral spectrum of the light beam off the target extracts features encoded in the wavefront topology, hence on the transversally-varying path length followed by the illuminating beam. Therefore, not only *intrinsic* but also *extrinsic* path length variations caused by physical, chemical, or biological processes are susceptible to be probed by this technique.

The details of the experimental implementation of the scheme put forward here depend on the concrete setting considered, e.g., whether implemented in reflection or in transmission; precise location and size of the detectors; corrections due to diffraction; etc. However, notice that suitable techniques to generate, to filter and to manipulate individual spiral harmonics are known in the form of combinations of holographic components and single-mode optical fibers. Importantly from a practical point of view, such components can be made in compact form using currently available micro-optics fabrication technologies [21, 22].

#### 4. Conclusions

We thus conclude stressing the feasibility of our concept, and its applicability to different bands across the electromagnetic spectrum. The phase and amplitude features shown here are intended only as *canonical* examples to illustrate the potential of the imaging technique. However, notice that they might have direct applications, e.g., in compact disc technologies for optical storage

[23], and for serial biosensing [24].

While the high sensitivity of the scheme advanced here to phase and amplitude variations might pose restrictions on its practical applicability in turbid or in disordered media, it might likewise be used to gain information about the random properties of the corresponding light path. Finally, notice that the concept of digital spiral imaging can also be extended to non-paraxial light beams and to their corresponding spiral spectra.

### **Acknowledgments**

This work was supported by the NOMSAN (Novel Optical Methods for Self-Assembled Nanostructures) program of the European Science Foundation, by the Generalitat de Catalunya, by grant number BFM2002-2861 from the Government of Spain; and by the Fulbright Program and the Ministry of Education and Science of the Government of Spain.